Available online at www.sciencedirect.com
SCIENCE DIRECT®
Remote Sensing of Environment 88 (2003) 442–452
Remote Sensing of Environment
www.elsevier.com/locate/rse

Modeling seasonal changes in live fuel moisture and equivalent water thickness using a cumulative water balance index

Philip E. Dennison[a,*], Dar A. Roberts[a], Sommer R. Thorgusen[b], Jon C. Regelbrugge[c], David Weise[d], Christopher Lee[e]

[a] Department of Geography, University of California, Santa Barbara, CA 93106, USA
[b] Department of Geography, University of Arizona, Tucson, AZ 85721, USA
[c] San Jacinto Ranger District, San Bernardino National Forest, USDA Forest Service, San Bernardino, CA 92408, USA
[d] Riverside Forest Fire Lab, USDA Forest Service, Riverside, CA 92507, USA
[e] Department of Geography, California State University Long Beach, Long Beach, CA 90840, USA

Received 29 April 2003; received in revised form 29 July 2003; accepted 18 August 2003

Abstract

Live fuel moisture, an important determinant of fire danger in Mediterranean ecosystems, exhibits seasonal changes in response to soil water availability. Both drought stress indices based on meteorological data and remote sensing indices based on vegetation water absorption can be used to monitor live fuel moisture. In this study, a cumulative water balance index (CWBI) for a time series spanning 1994–1997 and 1999–2001 was compared to field measured live fuel moisture and to equivalent water thickness (EWT) calculated from remote sensing data. A sigmoidal function was used to model the relationships between CWBI, live fuel moisture, and EWT. Both live fuel moisture and EWT reach minima at large CWBI deficits. Minimum and maximum live fuel moisture, minimum and maximum EWT, and the modeled inflection points of both live fuel moisture and EWT were found to vary with vegetation type. Modeled minimum and maximum EWT were also found to vary with vegetation biomass. Spatial variation in modeled EWT inflection points may be due to vegetation type and to local variation in soil moisture. Based on their temporal and spatial attributes, CWBI and EWT offer complimentary methods for monitoring live fuel moisture for fire danger assessment.

Keywords: Live fuel moisture; Equivalent water thickness; Cumulative water balance index

1. Introduction

Live fuel moisture is an important parameter for determining fire danger in Southern California. Southern California possesses a Mediterranean climate that is characterized by variable winter precipitation and prolonged summer drought. Decreases in vegetation moisture that accompany the seasonal decrease in available soil moisture can produce severe fire danger when low fuel moisture is combined with Santa Ana winds (Pyne, Andrews, & Laven, 1996). Live fuel moisture is particularly important for determining the behavior of fires in chaparral. Chaparral species possess flammable structure and chemistry that readily allow live canopy fuels to propagate wildfire (Philpot, 1977). Live fuel moisture in chaparral is typically measured using labor-intensive vegetation sampling (Countryman & Dean, 1979). Temporal and spatial characterization of live fuel moisture using meteorological and remote sensing data could greatly contribute to the monitoring of fire danger in southern California chaparral ecosystems.

2. Background

The Keetch Byram Drought Index (KBDI) was developed to measure cumulative soil water deficits in forested ecosystems to assess fire potential (Keetch & Byram, 1968). KBDI utilizes precipitation and maximum temperature to estimate the net effect of daily precipitation and evapotranspiration on soil water balance. KBDI assumes a soil water

* Corresponding author. Tel.: +1-805-893-4434; fax: +1-805-893-3146.
E-mail address: dennison@geog.ucsb.edu (P.E. Dennison).

0034-4257/$ - see front matter © 2003 Elsevier Inc. All rights reserved.
doi:10.1016/j.rse.2003.08.015

capacity of approximately 20 cm, and that moisture is lost exponentially from the soil reservoir. KBDI is calculated as

$$\mathrm{KBDI}_t = \mathrm{KBDI}_{t-1} + \frac{[203.2-(\mathrm{KBDI}_{t-1}-P_t)][0.968\mathrm{e}^{(0.0875T_{\max}+1.5552)}-8.30]}{1+10.88\mathrm{e}^{-0.001736P_a}} \times 10^{-3} \quad (1)$$

where t is the time interval of 1 day, P_t is the precipitation for day t in millimeters, $T_{\max}$ is the maximum temperature for day t in degrees Celsius, and P_a is the mean annual precipitation in millimeters (Dimitrakopoulos & Bemmerzouk, 2003; Keetch & Byram, 1968). The United States Department of Agriculture Forest Service uses KDBI as a component of the National Fire Danger Rating System (NFDRS). In the NFDRS, KDBI is used to estimate the amount of dead fuel available for combustion (Burgan, 1988).

In addition to dead fuel moisture, KDBI has also been linked to live fuel moisture. Live fuel moisture describes the water content of herbaceous and small woody vegetation as a percentage of the dry weight:

$$M = \frac{m_w - m_d}{m_d} \quad (2)$$

where M is the live fuel moisture, m_w is the measured mass of the wet fuel, and m_d is the measured mass of the dried fuel. Dimitrakopoulos and Bemmerzouk (2003) demonstrated a strong relationship between KDBI and live fuel moisture for herbaceous understory vegetation in a Mediterranean pine forest.

Dennison and Roberts (2003) introduced a simple index for measuring regional drought stress. The cumulative water balance index (CWBI) cumulatively sums precipitation and reference evapotranspiration over time so that the CWBI at time T is calculated as

$$\mathrm{CWBI}_T = \sum_{t=0}^{T}(P_t - \mathrm{ET}_{0t}) \quad (3)$$

where t is the time interval, P_t is the precipitation over each interval, and ET_{0t} is the reference evapotranspiration over each interval. In Dennison and Roberts, precipitation and reference evapotranspiration were measured at a California Irrigation Management Information System (CIMIS) station. CIMIS uses a modified Penman equation (Snyder & Pruitt, 1992) to calculate reference evapotranspiration using inputs of solar irradiance, air temperature, vapor pressure, and wind speed. Functionally, CWBI is very similar to KBDI, and relationships between live fuel moisture and KDBI demonstrated by Dimitrakopoulos and Bemmerzouk (2003) should also apply to CWBI. CWBI has two important advantages over KBDI: (1) CWBI does not exponentially decay to an assumed maximum soil water deficit, as KBDI does, and (2) CWBI as implemented using CIMIS data relies on several meteorological variables to model evapotranspiration, while KBDI uses only maximum daily temperature.

Remote sensing data provides a possible means for quantifying spatial differences in live fuel moisture. Remote sensing measures of vegetation moisture rely on liquid water absorption features in reflected visible and near-infrared solar radiation. Water index (WI; Peñuelas, Pinol, Ogaya, & Filella, 1997), normalized difference water index (NDWI; Gao, 1996), and equivalent water thickness (EWT; Gao & Goetz, 1995; Green, Conel, Margolis, Bruegge, & Hoover, 1991; Roberts, Brown, Green, Ustin, & Hinckley, 1998) and radiative transfer simulations (Jacquemoud et al., 1996; Zarco-Tejada, Rueda, & Ustin, 2003) have all been related to the relative water content of vegetation. WI and NDWI are band ratios that relate vegetation reflectance in water absorption features centered around 970 and 1200 nm to reflectance in reference bands located outside the absorption features. EWT is a measure of the thickness of water that would be required to mimic water absorption features in vegetation spectra. Serrano, Ustin, Roberts, Gamon, and Penuelas (2000) compared WI, NDWI, and EWT calculated from AVIRIS data to relative water content in Southern California chaparral. WI and NDWI accounted for most of the variation in canopy relative water content, but the relationship between these indices and relative water content was found to be species dependent. Peñuelas et al. (1997) used time series field spectrometer data to relate WI to the relative water content of Mediterranean plant seedlings. Jacquemoud et al. (1996) employed the PROSPECT leaf radiative transfer model to estimate several leaf biochemical components, including water content. Zarco-Tejada et al. (2003) used leaf- and canopy-level radiative transfer modeling to estimate EWT from MODIS data and demonstrated a correlation between EWT and field-measured live fuel moisture in Southern California chaparral.

Time series remote sensing data can be used to correlate water absorption indices and relative water content. Roberts, Green, and Adams, (1997) and Ustin et al. (1998) identified seasonal changes in EWT that are dependent on changes in vegetation moisture in chaparral. Since precipitation and evapotranspiration are seasonally and annually variable in Mediterranean ecosystems, relating remote sensing data from different years must rely on a measure of drought stress (Dennison & Roberts, 2003). CWBI is a relative measure of drought stress that can be used to relate live fuel moisture and EWT measurements occurring in different years. It is demonstrated here that CWBI can also be used to model temporal trends in live fuel moisture and EWT and spatial variation in the effects of regional drought stress on EWT.

3. Methods

3.1. Study area

Seasonal changes in live fuel moisture and remotely sensed EWT were examined in the Santa Monica Mountains, west of Los Angeles, California, USA (Fig. 1). The Santa Monica Mountains are an east–west-trending mountain range with elevation varying from sea level at the

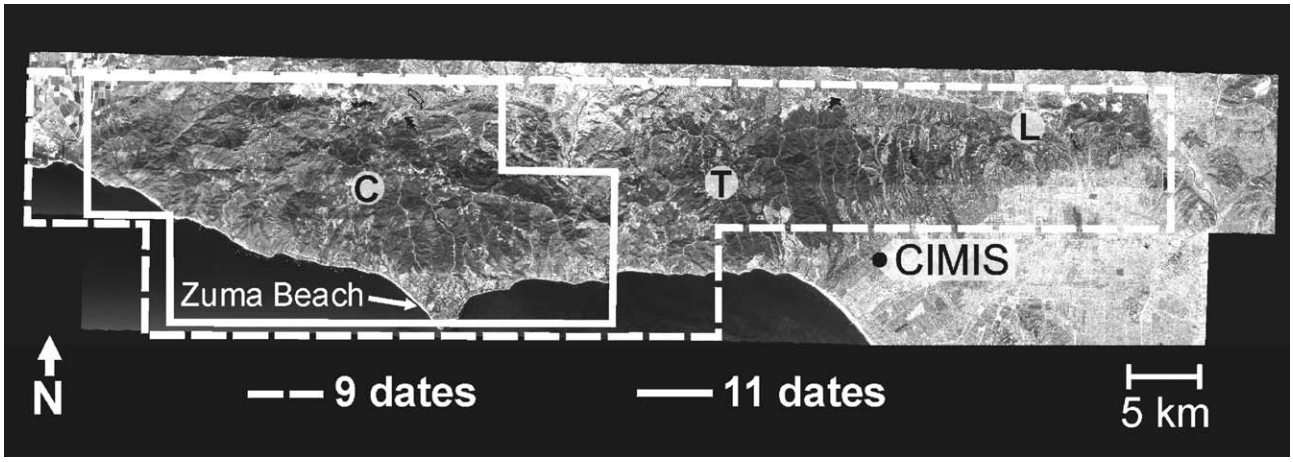

Fig. 1. AVIRIS time series coverage in the Santa Monica Mountains. The image shown is a mosaic of the 675-nm band extracted from two registered AVIRIS image swaths acquired on October 4, 1999. The Pacific Ocean is in the lower part of the figure, and the Los Angeles Basin is to the right. The lines indicate the area covered by at least 9 AVIRIS dates and by all 11 dates in the time series. The CIMIS station in Santa Monica is marked by the black dot. The approximate locations of the LACFD vegetation moisture sites are marked by C (Clark Motorway), T (Trippet Ranch), and L (Laurel Canyon).

Pacific Ocean to 948 m at Sandstone Peak (Fig. 2). Four vegetation communities are prevalent in the Santa Monica Mountains: grasslands, coastal sage scrub, chaparral, and riparian woodlands. Each of these vegetation communities has different strategies for dealing with drought stress. Introduced European grasslands and coastal sage scrub senesce during the dry season. Evergreen chaparral possesses thick sclerophyllous leaves that reduce moisture loss and is the most common plant community in the Santa Monica Mountains. Year-round water availability supports riparian vegetation in canyon bottoms.

3.2. CWBI

CWBI was calculated by cumulatively summing precipitation and reference evapotranspiration (Dennison & Roberts, 2003). Precipitation was measured at a CIMIS station in Santa Monica, CA, approximately 5 km from the Santa Monica Mountains at an elevation of 100 m (Fig. 1). Reference evapotranspiration (ET_0) was calculated using a modified Penman equation (Snyder & Pruitt, 1992) from solar irradiance, air temperature, vapor pressure, and wind speed measured at the same CIMIS station. CWBI was constrained to be positive until after the last substantial (>3 mm) precipitation of the year (Dennison & Roberts, 2003). For each date after the last rainfall, CWBI was calculated as a positive or negative sum of the seasonal precipitation and ET_0. The index was calculated daily for April 1–October 31 in 1994–1997 and 1999–2001. Unusually high runoff due to record rains associated with El Niño skewed the CWBI for 1998, so these data were not used. CWBI was compared to live fuel moisture measurements and to an EWT time series constructed from AVIRIS data.

3.3. Live fuel moisture

Live fuel moisture was sampled by the Los Angeles County Fire Department (LACFD) at three sites in the Santa Monica Mountains during the study period of 1994–2001. Data sampled at the Clark Motorway, Laurel Canyon, and Trippet Ranch sites were used in this study (Fig. 1). *Adenostoma fasciculatum* and *Ceanothus megacarpus* (big pod ceanothus) were sampled at the Clark Motorway site, *A. fasciculatum* was sampled at the Laurel Canyon site, and *A. fasciculatum* and *Salvia mellifera* (black sage) were sampled at the Trippet Ranch site at an interval of once every 2–3

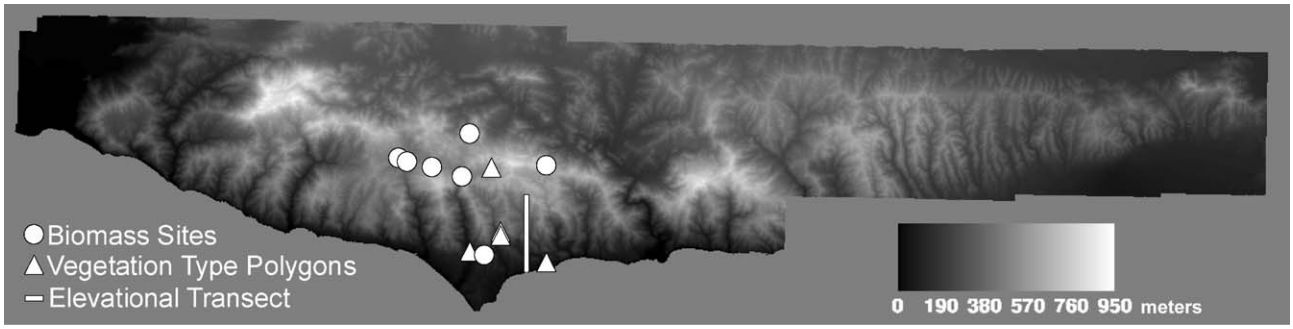

Fig. 2. Elevation in meters and the locations of biomass sites, vegetation type polygons, and the elevational transect in Fig. 7.

weeks throughout the year. Live fuel moisture was measured using methods developed by Countryman and Dean (1979) for chaparral vegetation. Live samples consisting of leaves and stems less than 3.2 mm (1/8 in.) in diameter were collected and weighed. The samples were then dried to remove water from the samples and reweighed to calculate live fuel moisture.

3.4. EWT

EWT was calculated for a time series of registered imaging spectrometry data acquired by AVIRIS onboard a NASA high-altitude ER-2 platform using methods described by Green, Conel, and Roberts (1993) and Roberts et al. (1997). AVIRIS is a 224-band imaging spectrometer that covers a spectral range of 400–2500 nm, has a swath width of approximately 11 km, and has an instantaneous field of view (IFOV) of approximately 20 m (Green et al., 1998). AVIRIS data were acquired over the Santa Monica Mountains on 11 dates from 1994 to 2001 (Table 1). All acquisition dates were during the dry season, typically lasting from April to November, and represent a wide range of vegetation drought stress as quantified by CWBI (Table 1). Six acquisition dates occurred during the month of October, and the remaining acquisition dates were in April, May, and June. Solar zenith was closely related to the date of acquisition, with the lowest solar zeniths occurring in April, May, and June. Solar zenith ranged from 12.2° for the June 6, 2000 acquisition to 46.5° for the October 26, 1995 acquisition (Table 1).

Two east–west AVIRIS image swaths were required to completely cover the study area. Spatial rectification of the AVIRIS image swaths was the most challenging component of time series construction. Terrain displacement was significant in all mountainous areas as a result of the aerial platform. The October 1999, June 2000, and June 2001 AVIRIS scenes were corrected for geometric distortions due to aircraft motion by the Jet Propulsion Laboratory. The remaining eight dates all contained some amount of distortion due to aircraft motion. Terrain displacement and geometric distortions were corrected using control point registration and image warping by triangulation. Each of the 22 image swaths was registered to an orthorectified SPOT mosaic resampled to a resolution of 20 m. A total of 12,955 control points were used to register the 22 image swaths.

Table 1
The dates and solar zenith angles of 11 AVIRIS acquisitions over the Santa Monica Mountains

AVIRIS date	Solar zenith (°)	CWBI (cm)
11 April 1994	26.8	−3.0
19 October 1994	43.7	−76.2
9 May 1995	25.3	+23.6
20 October 1995	45.4	−41.5
26 October 1995	46.5	−43.2
23 October 1996	45.7	−37.2
7 April 1997	27.5	+15.2
3 October 1997	37.7	−64.7
4 October 1999	38.4	−49.2
6 June 2000	12.2	−20.2
27 June 2001	24.5	−12.8

CWBI calculated for each AVIRIS date is also shown.

AVIRIS data were processed to apparent surface reflectance using a modified version of the MODTRAN3 radiative transfer model (Green et al., 1993, Roberts et al., 1997). Given a solar zenith angle and atmospheric visibility for each AVIRIS scene, MODTRAN3 was used to generate look-up tables for path radiance and reflected radiance for a range of water vapor values. Modeled radiance was fit to measured at-sensor radiance using a nonlinear least squares fitting routine (Green et al., 1993; Roberts et al., 1997). After the initial reflectance retrieval, the reflectance data were adjusted using field spectrometer measurements from Zuma Beach (Fig. 1) (Clark, Swayze, Heidebrecht, Goetz, & Green, 1993). Field spectrometer measurements were taken in 1995, 1997, and 1998 using an Analytical Spectral Devices Full Range Field Spectrometer (ASD, Boulder, CO, USA).

EWT was calculated from the reflectance data by fitting the spectral region from 850 to 1100 nm with a water absorption model. Reflectance (ρ_λ) was modeled as a linear function of wavelength (λ) multiplied by an absorption function:

$$\rho_\lambda = (m\lambda + b)e^{-t\alpha_\lambda} \quad (4)$$

where m and b are coefficients that determine the slope and intercept of the linear function, α_λ is the absorption coefficient of liquid water, and t is the equivalent water thickness (Gao & Goetz, 1995; Green, 2003; Roberts et al., 1997). Eq. (4) was fit to each reflectance spectrum in the time series using a nonlinear least squares fitting routine. EWT images were warped using the set of registration points for each date and resampled to a uniform spatial resolution of 20 m using nearest neighbor resampling. The resulting registered EWT time series covers a land area in excess of 1400 km^2, with 850 km^2 covered by at least 9 dates and nearly 400 km^2 covered by all 11 dates (Fig. 1).

3.5. Modeling

Both the live fuel moisture time series and the EWT time series exhibited apparent minima at higher drought stress, as measured by CWBI. Based on these trends, a sigmoidal function was used to model the relationship between CWBI and the two time series. Sigmoidal functions have previously been used to model temporal changes in vegetation indices responding to early season greening of croplands (Badhwar, 1984) and the phenology of eastern US forests (Zhang et al., 2003). The model function is defined by

$$R = a + \frac{b}{1 + e^{-(c+d\mathrm{CWBI})}} \quad (5)$$

where R is the vegetation response (measured as live fuel moisture or EWT). Parameter a defines the base level

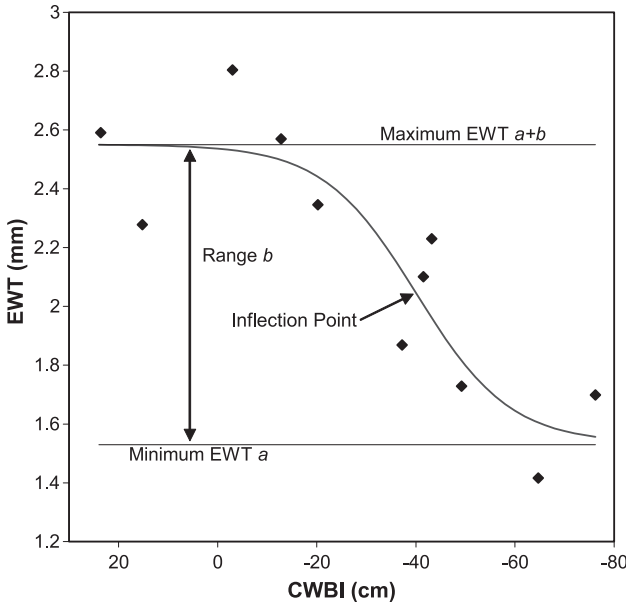

Fig. 3. Important parameters in the sigmoidal model include the minimum response (a), the response range (b), the maximum response ($a+b$), and the inflection point. The sigmoidal fit to an EWT time series pixel containing chaparral is shown.

response at large CWBI deficits and is the minimum response as long as the response (live fuel moisture or EWT) decreases with CWBI (Fig. 3). Parameter b defines the range between the minimum and maximum response and is positive if the response decreases with CWBI (Fig. 3). Parameters c and d control the timing and slope of the sigmoidal function.

The sigmoidal function was fit to live fuel moisture and two EWT using nonlinear least squares. In the case of the live fuel moisture data, between 79 and 90 points relating live fuel moisture and CWBI were fit using the sigmoidal function. In the case of the EWT data, each 20-m pixel possessed between 9 and 11 EWT values from the EWT time series and a constant CWBI for each date. For the EWT time series, a was constrained to be greater than the minimum EWT in the pixel, and b was constrained to be less than the difference between the minimum and maximum EWT in the pixel.

For both time series, the slope (dR/dCWBI) of the best-fit sigmoidal function was calculated using the first derivative of the sigmoidal function:

$$\frac{dR}{\mathrm{dCWBI}} = \frac{bde^{-(c+d\mathrm{CWBI})}}{(1+e^{-(c+d\mathrm{CWBI})})^2} \quad (6)$$

The maximum value of the derivative function indicates the maximum slope, which occurs at the inflection point of the sigmoidal function. The inflection point, as measured in CWBI units (cm), was used to quantify the timing of the maximum decrease in the modeled function (Fig. 3). Vegetation that has an early seasonal change in live fuel moisture or EWT in response to drought stress should have a positive or small negative inflection point, while vegetation that has a late seasonal change in live fuel moisture or EWT in response to drought stress should have a large negative inflection point in terms of CWBI.

3.6. Vegetation type and biomass data

Sims and Gamon (2003) demonstrated that water absorption in Southern California vegetation is dependent on vegetation type and leaf area index (LAI). To determine whether parameters of the sigmoidal functions fit to the EWT time series were influenced by vegetation type and biomass, fit parameters were compared to field data. Polygons for chaparral, coastal sage scrub, and grassland land cover types were delineated using field inspection and a 1-m resolution United States Geological Survey (USGS) Digital Orthophoto Quadrangle (DOQ). Approximate locations of the polygons are shown in Fig. 2. The polygons for chaparral and coastal sage scrub were located within 100 m of each other. The grassland polygon was located at a lower elevation coastal site. Two additional vegetation type polygons containing irrigated orchard trees were also delineated using the DOQ to examine possible effects of solar zenith angle on EWT. There is a weak linear relationship between solar zenith angle and CWBI for the AVIRIS scenes used in the time series ($R^2 = 0.44$). Solar zenith angles in the time series were smallest in AVIRIS scenes with positive CWBI values and largest in AVIRIS scenes with negative CWBI values (Table 1). Since the orchards are irrigated, EWT extracted from orchard pixels should have a poor relationship with CWBI.

Seven biomass sites were harvested in the Santa Monica Mountains in 1995 and 1996 (Table 2). For six stands dominated by *A. fasciculatum* and *C. megacarpus*, three 4×4-m plots were randomly located within the stand, and live leaf and stem materials were harvested. A seventh stand dominated by *Salvia leucophylla* (purple sage) was harvested using three 2 meter by 2 meter randomly located plots. The components of the harvested shrubs were

Table 2
Santa Monica Mountains biomass harvest sites

Site name	Dominant species	Age (years)	Mean elevation (m)	Aboveground live biomass (Mg/ha)	Number of AVIRIS pixels
c13c	*Adenostoma fasciculatum*	40	464	22.4	18.0
c13m	*Ceanothus megacarpus*	18	410	48.2	31.0
ccn	*Adenostoma fasciculatum*	13	595	25.1	7.0
kt	*Ceanothus megacarpus*	17	509	72.0	8.0
lkw	*Salvia leucophylla*	14	172	11.4	8.0
rom	*Ceanothus crassifolius*	17	573	77.1	41.0
zr	*Adenostoma fasciculatum*	17	564	25.3	15.0

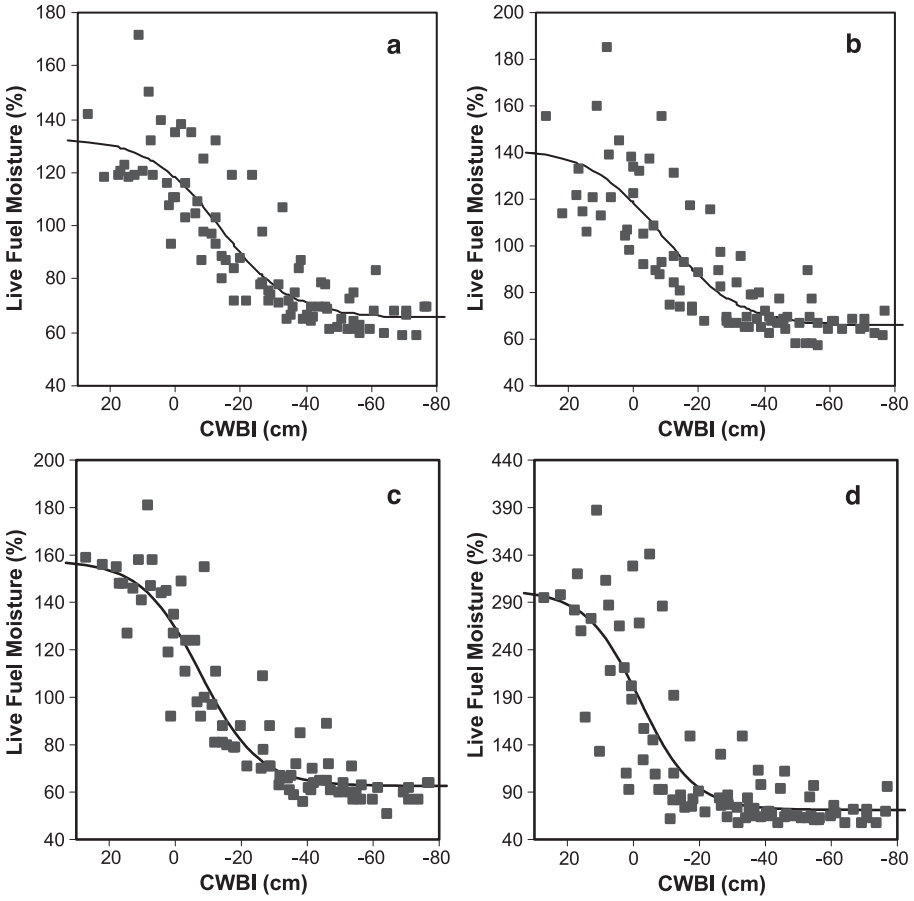

Fig. 4. CWBI versus live fuel moisture, as a percent of dry weight, for LACFD measurements spanning 1994–1997 and 1999–2002. The 1998 measurements are excluded due to high runoff. Model fits are shown for (a) *A. fasciculatum* at the Clark Motorway site, (b) *A. fasciculatum* at the Trippet Ranch site, (c) *C. megacarpus* at Clark Motorway, and (d) *S. mellifera* at Trippet Ranch.

weighed, and a subsample was weighed and then dried to remove moisture. The dried mass of the subsample was used to calculate the dry biomass of the entire plot, and values for the plots were averaged to the stand level.

4. Results

4.1. Live fuel moisture

Live fuel moisture demonstrated a strong, nonlinear relationship with CWBI. The live fuel moisture data for four LACFD samples are shown in Fig. 4. The plot for Laurel Canyon *A. fasciculatum* was similar to those shown and was omitted. High CWBI values coincide with high spring live fuel moisture levels. As CWBI decreased from surplus to deficit, live fuel moisture steeply declined. Between CWBI values of −20 and −40 cm, live fuel moisture leveled out and reached a minimum that ranged between 60% and 80% live fuel moisture for each site. Despite differences in vegetation species, sampling location, and seasonal rainfall, this minimum moisture level was consistent from year to year. *S. mellifera* sampled at Trippet Ranch (Fig. 4d) had the widest range in sampled

Table 3
Model fits to the LACFD live fuel moisture time series

Site	Elevation (m)	Minimum moisture *a* (%)	Maximum moisture (%)	Range *b* (%)	*c*	*d*	Inflection point (cm)	RMSE (%)
Clark *adfa*	430	65.5	133.0	67.5	1.26	0.09	−13.7	12.6
Laurel *adfa*	370	72.0	113.4	41.5	1.77	0.14	−13.1	15.7
Trip *adfa*	310	65.6	142.2	76.5	0.79	0.09	−9.1	15.7
Clark *ceme*	430	62.6	157.6	95.0	0.85	0.11	−7.6	12.6
Trip *same*	310	71.3	302.9	231.6	0.23	0.12	−1.9	46.9

The samples included in the time series are Clark Motorway *A. fasciculatum*, Laurel Canyon *A. fasciculatum*, Trippet Ranch *A. fasciculatum*, Clark Motorway *C. megacarpus*, and Trippet Ranch *S. mellifera*.

moisture values, ranging from nearly 390% to below 60%. *C. megacarpus* sampled at Clark Motorway (Fig. 4c) displayed slightly higher spring moisture than *A. fasciculatum* sampled at Clark Motorway (Fig. 4a) or Trippet Ranch (Fig. 4b).

Live fuel moisture was fit against CWBI using Eq. (5). The parameters of these model fits are shown in Table 3. The Clark Motorway samples possessed the best fits, with an RMSE of 12.6% live fuel moisture for both *A. fasciculatum* and *C. megacarpus*. *S. mellifera* sampled at Trippet Ranch, which had more variability in moisture and a higher moisture range, also had the poorest fit with an RMSE of 46.9%. The modeled minimum moisture (a) was between 62.6% and 72.0% for all three sampled species. *S. mellifera* possessed a modeled moisture range of over 230%, more than twice that of any of the *A. fasciculatum* and *C.*

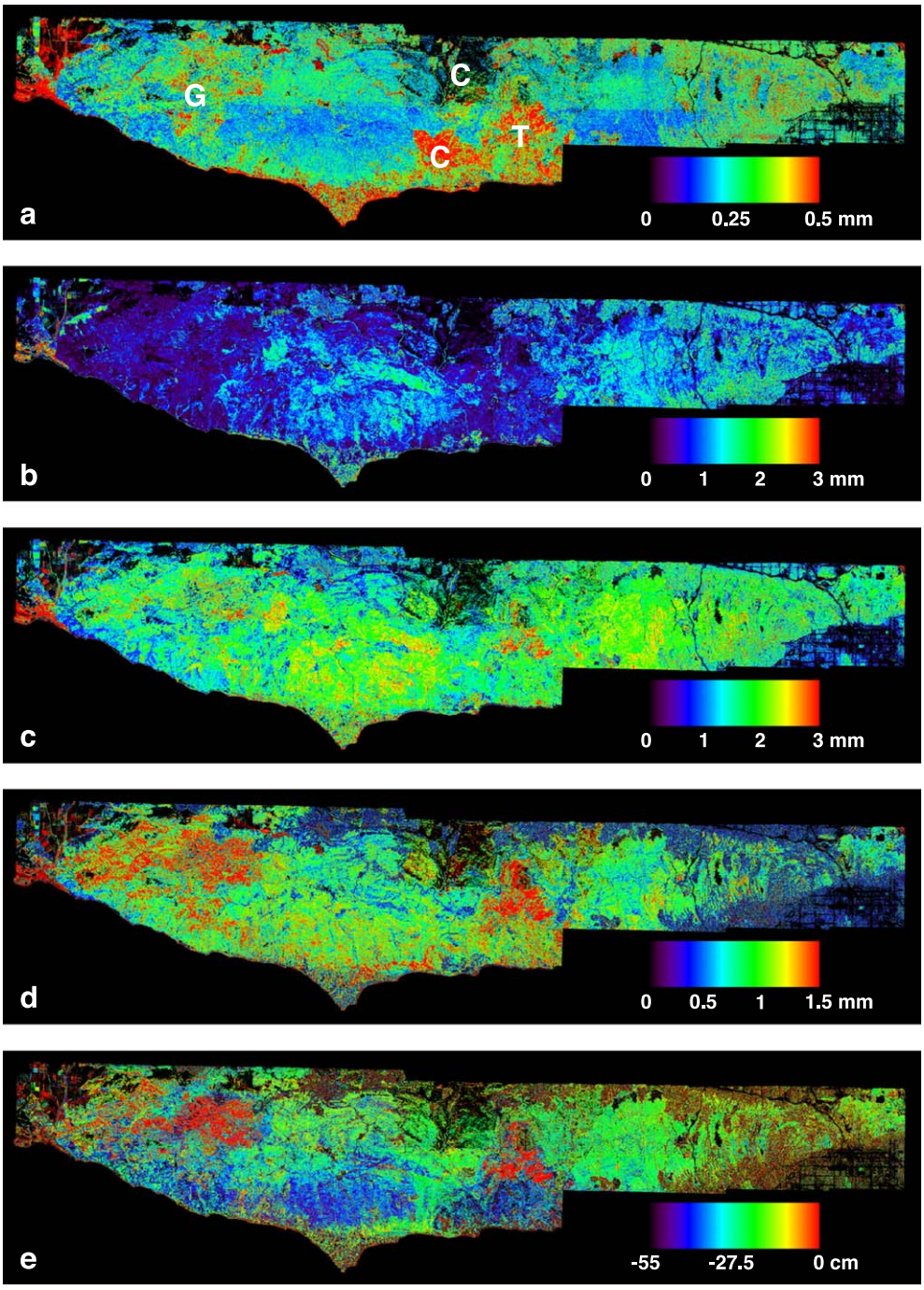

Fig. 5. Image model fit parameters for the EWT time series, including (a) RMSE, (b) minimum EWT, (c) maximum EWT, (d) EWT range, and (e) CWBI inflection point. Fire scars are marked in the RMSE image as the 1993 Green Meadow Fire (G), the 1993 Topanga Fire (T), and the northern and southern halves of the 1996 Calabasas Fire (C).

megacarpus samples. The modeled inflection points also demonstrated differences between species (Table 2). *S. mellifera* showed the earliest decline in moisture, with an inflection point of −1.9 cm CWBI. The *C. megacarpus* inflection point occurred at −7.6 cm CWBI. The inflection points for the three *A. fasciculatum* occurred at the largest soil water deficits, with inflection points at −9.1, −13.1, and −13.7 cm CWBI.

4.2. EWT

Eq. (5) was fit to each 20-m resolution EWT time series pixel and the CWBI calculated for each date to create images of fit parameters (Fig. 5). RMSE of the model fits was below 0.3 mm EWT in most naturally vegetated areas (Fig. 5a). RMSE was uniformly higher in the northern half of the Santa Monica Mountains due to higher variability in apparent surface reflectance within the 970-nm water absorption band. Both the northern and southern AVIRIS swaths were calibrated based on the spectrum from a target in the southern AVIRIS swath. Differences in atmospheric scattering and water vapor absorption between the northern and southern swaths produce higher variability in EWT in the northern swath. Model fits were poorest in pixels with temporal vegetation disturbances such as wildfire and human activity. The fire scars from the 1993 Green Meadow Fire (G), 1993 Topanga Fire (T), and 1996 Calabasas Fire (C) all possessed RMSE in excess of 0.3 mm EWT (Fig. 5a). For the 1993 fires, vegetation was recovering during the period of the EWT time series, creating an increase in EWT with time and reducing the seasonal correlation with CWBI. Effects from the 1996 Calabasas Fire are readily apparent in the time series, since the time series contains both pre- and post-fire measures of vegetation abundance and moisture. The nonlinear least squares fitting routine was unable to fit the data over much of the northern half of the Calabasas Fire, shown in black (Fig. 5). While the fire scars may create difficulties for monitoring vegetation water stress, time series EWT may be valuable for quantifying post-fire recovery. Crops grown in the Oxnard Plain, at the far left of Fig. 5a, do not share the seasonality of natural vegetation and thus have a high RMSE. Human disturbance such as residential development also creates poor model fits in a few areas in the northern half of the image.

Table 5
z-test results testing for the significance of differences in model parameters between vegetation types

Sample pair	Minimum EWT *a* (mm)	Maximum EWT (mm)	EWT range *b* (mm)	Inflection point (CWBI, cm)
Grass and CSS	**4.24**	**3.53**	*1.97*	**7.00**
Grass and chaparral	**42.15**	**19.15**	0.97	**10.99**
CSS and chaparral	**5.56**	**19.55**	*1.66*	**5.02**

Values significant at $\alpha = 0.01$ are bold, and values significant at $\alpha = 0.05$ are italicized.

Modeled minimum EWT (Fig. 5b) and maximum EWT (Fig. 5c) define the baseline and upper limit canopy water absorption. The modeled minimum and maximum EWT values are highest in high-elevation areas outside of the fire scars. Modeled range (Fig. 5d) was highest within the fire scars and in low-elevation vegetated areas close to the Pacific Ocean. For most natural vegetation types, the modeled range was close to 1 mm EWT. The range in EWT was smallest in residential areas surrounding the Santa Monica Mountains. The modeled inflection points demonstrated several important spatial trends (Fig. 5e). The most rapid change in EWT occurred at small negative CWBI values in lower elevation grassland and chaparral areas in the northern and eastern Santa Monica Mountains (Fig. 5e). Inflection points occurred at more negative CWBI values in higher elevation, inland areas of the Santa Monica Mountains.

Model parameters extracted from the vegetation type polygons demonstrate significant differences in minimum and maximum EWT, range, and inflection points (Table 4). Maximum EWT was lowest for the grassland polygon and highest for the chaparral and orchard polygons. Similarly, modeled minimum EWT was lowest for the grassland polygon and highest for the chaparral and orchard polygons. The grassland and chaparral vegetation types exhibited the largest range in EWT at 1.09 and 1.04 mm EWT, respectively. Mean RMSE for grass, coastal sage scrub, and chaparral polygons ranged from 0.23 to 0.27 mm EWT (Table 4). Mean inflection points also varied with vegetation type. The inflection point for grassland occurred at the least negative CWBI value, while the inflection point for chaparral occurred at the most negative CWBI value.

Table 4
Model fits to vegetation type polygons from the EWT time series

Vegetation type	Number of pixels	Mean elevation (m)	Minimum EWT *a* (mm)	Maximum EWT (mm)	EWT range (mm) *b*	*c*	*d*	Inflection point (CWBI, cm)	RMSE (mm EWT)
Grass	43	67	0.24	1.34	1.09	14.2	0.78	−1.5	0.24
CSS	61	299	0.80	1.59	0.79	19.2	0.62	−27.3	0.27
Chaparral	115	247	1.55	2.58	1.04	16.5	0.43	−37.8	0.23
Orchard	147	30/500	2.45	2.56	0.12	6.0	0.36	−9.9	0.52

EWT extracted from the orchard polygons was not directly related to solar zenith angle. A linear regression between EWT and solar zenith angle by date produced an average R^2 of 0.14 and a slope near zero. RMSE values from the sigmoidal model fit of orchard EWT and CWBI were high, with a mean RMSE 0.52 mm EWT (Fig. 4). The mean range in EWT for the orchard polygons was very low at 0.12 mm; however, this value is somewhat misleading. 101 of the 147 pixels within the orchard polygons were modeled with a decrease in EWT as CWBI decreased, so that the range, b, was positive. The remaining 46 pixels were modeled with a negative b, so that EWT increased as CWBI decreased. Since no clear relationship was found between solar zenith angle and EWT for the orchard, solar zenith angle effects on EWT are likely minor.

The statistical significance of the differences in fit parameters between the chaparral, coastal sage scrub, and grassland polygons was evaluated using a two-tailed z-test (Devore, 2000). The statistic z was calculated as

$$z = \frac{\bar{x}_1 - \bar{x}_2}{\sqrt{\frac{s_1^2}{n_1} + \frac{s_2^2}{n_2}}} \quad (7)$$

where $\bar{x}$ is the mean of polygons 1 and 2, s is the standard deviation of polygons 1 and 2, and n is the number of pixels in each polygon. Results of the z-test are shown in Table 5. Differences in the minimum and maximum EWT and mean inflection points were all found to be significant, at a significance level (α) of 0.01. Differences in mean range were significant at $\alpha = 0.05$ for grasslands and coastal sage scrub and for chaparral and coastal sage scrub.

Model parameters were also related to biomass measured at the seven biomass harvest sites (Table 6). Both the minimum and maximum EWT model parameters increased with increasing biomass. Fig. 6 shows the linear regression between aboveground live biomass and the minimum and maximum EWT for each site. Both regressions had similar slopes, but the intercept for the maximum EWT points was 0.87 mm higher than the intercept for the minimum EWT points. The minimum EWT points possessed the strongest linear correlation with biomass, with an R^2 of 0.88. Range and inflection point do not appear to be related to biomass (Table 6). The single coastal sage scrub biomass site possessed an inflection point with a less negative CWBI than that of the six chaparral sites, validating the differences in inflection points seen in the vegetation type polygons.

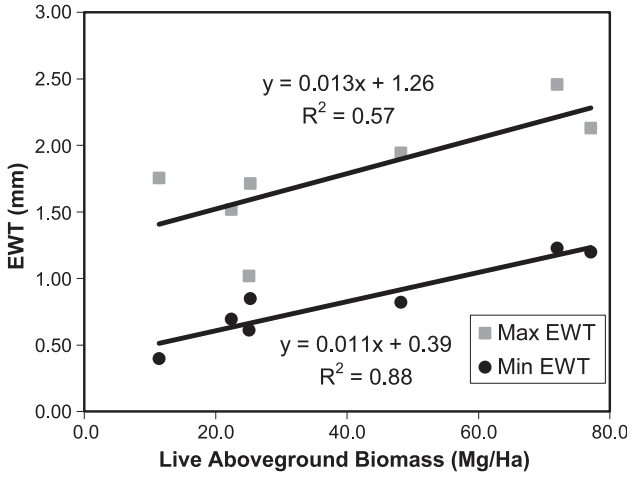

Fig. 6. Live aboveground biomass versus the minimum and maximum EWT parameters extracted from the modeled EWT time series using the biomass polygons.

5. Discussion

Using a CWBI calculated at a single point to fit EWT over the entire Santa Monica Mountains reveals spatial differences in the modeled inflection point. The timing of the inflection points was demonstrated to vary by vegetation type. Evergreen chaparral possessed inflection points with the largest CWBI deficits for both the live fuel moisture samples and the EWT time series. Inflection points for the drought senescent vegetation types, grassland and coastal sage scrub, occurred at small CWBI deficits. Since CWBI is calculated for a single point, it does not account for local variation in drought stress caused by variable precipitation and evapotranspiration.

Conditions that may impact local drought stress include increased precipitation at higher elevations, spatial differences in moisture and solar insulation due to summer fog along the Pacific Coast, and soil depth and water capacity. The biogeography of vegetation communities is dependent on many of these same factors; thus, separating local varia-

Table 6
Model parameters for the seven biomass points

Site name	Biomass (Mg/ha)	Number of AVIRIS pixels	Minimum EWT a (mm)	Maximum EWT b (mm)	EWT range b (mm)	c	d	Inflection point (CWBI, cm)	RMSE (mm EWT)
lkw	11.4	8.0	0.40	1.75	1.36	2.8	0.27	− 7.9	0.23
c13c	22.4	18.0	0.70	1.52	0.82	12.8	0.57	− 16.2	0.17
ccn	25.1	7.0	0.61	1.02	0.41	46.3	1.16	− 33.0	0.20
zr	25.3	15.0	0.85	1.71	0.86	13.8	0.43	− 30.8	0.16
c13m	48.2	31.0	0.82	1.94	1.12	3.5	0.13	− 28.0	0.18
kt	72.0	8.0	1.23	2.46	1.23	10.9	0.42	− 28.1	0.16
rom	77.1	41.0	1.20	2.13	0.93	15.9	0.63	− 26.3	0.28

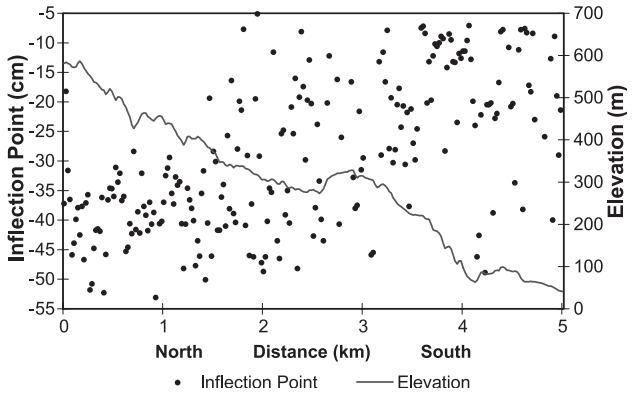

Fig. 7. A transect, from north to south, of elevation and modeled inflection point for the EWT time series. The location of the transect is shown in Fig. 2.

tion in drought stress from differences in vegetation land cover requires more detailed knowledge of land cover as well as multiple measurements of precipitation and evapotranspiration. A weak inverse relationship between the modeled inflection points and elevation is visible in a north–south transect of the southern slope of the Santa Monica Mountains. (Fig. 7). Elevation decreases from north to south, while the modeled inflection point increases over the same distance.

The modeled inflection points for the live fuel moisture time series occurred at much smaller CWBI deficits than the modeled inflection points for the EWT time series. For *S. mellifera*, the live fuel moisture inflection point of − 1.9 cm occurred earlier in the dry season than the EWT inflection points for the coastal sage scrub polygon (− 27.3 cm) and the *S. leucophylla* biomass site (− 7.9 cm). Similarly, the live fuel moisture inflection point for *C. megacarpus* occurred at − 7.6 cm, but the EWT inflection points for biomass sites containing *C. megacarpus* were approximately − 28 cm. While live fuel moisture and EWT have similar responses to drought stress as measured by CWBI, the timing of the inflection point for each of these variables appears to be different.

There are several factors that could contribute to the observed differences in modeled inflection points. The EWT time series did not have equal coverage of the full range of CWBI. Only two AVIRIS scenes were within the range of small CWBI deficits where the inflection points of the live fuel moisture and EWT data were modeled to have occurred in all vegetation types. Large CWBI deficits were overrepresented in the EWT time series, and the distribution of AVIRIS dates may have shifted inflection points from small CWBI deficits to larger CWBI deficits. The sensitivity of EWT to changes in vegetation water content must also be examined. Seasonal changes in live herbaceous biomass (leaf drop and senescence) may have produced a decrease in EWT without impacting the live fuel moisture of the remaining live materials. Riggan, Goode, Jacks, and Lockwood (1988) found a seasonal decrease in LAI in two *Ceanothus* species. The LAI of *Ceanothus crassifolius* decreased from 3.1 to 2.2, while the LAI of *Ceanothus oliganthus* decreased from 6.6 to 1.7. Neither of these species is dominant in the Santa Monica Mountains, but field observations indicate that *C. megacarpus*, while not experiencing the extreme change in LAI of *C. oliganthus*, does exhibit a decrease in LAI. If the most rapid fuel moisture changes occur prior to leaf drop, EWT may continue to decrease after live fuel moisture has reached a minimum value.

6. Conclusions

CWBI has value as a regional measure of drought stress, as demonstrated through its relationship with live fuel moisture and EWT. CWBI can be easily calculated using meteorological station data, permitting daily estimation of drought stress. When CWBI was used to model live fuel moisture data, the timing of inflection points in live fuel moisture varied by vegetation species. When CWBI was used to model time series EWT data, inflection points, minimum EWT and maximum EWT were all found to vary by vegetation type, while minimum and maximum EWT varied with biomass as well.

CWBI and remote sensing water absorption measures present complimentary methods for monitoring live fuel moisture in Southern California. CWBI has high temporal resolution, while remote sensing data has superior spatial coverage. CWBI could be calculated for CIMIS stations across California and for other remote automated weather stations present in many fire-prone ecosystems. CWBI calculated from these data could be combined with 500-m resolution MODIS NDWI (Gao, 1996) to intensively monitor live fuel moisture both temporally and spatially, without the need for vegetation sampling.

Acknowledgements

The authors would like to acknowledge the undergraduates at California State University Long Beach who assisted with the registration of several AVIRIS image swaths, the Los Angeles County Fire Department and Herb Spitzer for providing the live fuel moisture data, and the Jet Propulsion Laboratory for providing the AVIRIS data. We also thank the reviewers for their helpful comments. Support for this research was provided by a National Aeronautics and Space Administration (NASA) Earth Systems Science Fellowship (NGT5-50327), and the NASA Solid Earth and Natural Hazards (NAG2-1140), Regional Earth Science Application Center (CSDH NASA RESAC 447633-59075), and EO-1 Science Validation (NCC5-496) programs.

References

Badhwar, G. B. (1984). Automatic corn–soybean classification using Landsat MSS Data: II. Early season crop proportion estimation. *Remote Sensing of Environment*, *14*, 31–37.

Burgan, R. E. (1988). *1988 Revisions to the 1978 national fire-danger rating system*. Asheville, NC: US Dept. of Agriculture, Forest Service Research Paper SE-273, Southeastern Forest Experiment Station.

Clark, R. N., Swayze, G., Heidebrecht, K., Goetz, A. F. H., & Green, R. O. (1993). Comparison of methods for calibrating AVIRIS data to ground reflectance. *Summaries of the 4th Annual JPL Airborne Geoscience Workshop* (pp. 35–36). Pasadena, CA: Jet Propulsion Laboratory.

Countryman, C. M., & Dean, W. A. (1979). *Measuring moisture content in living chaparral: A field user's manual*. Berkeley, CA: U.S. Dept. of Agriculture, Forest Service, Pacific Southwest Forest and Range Experiment Station.

Dennison, P. E., & Roberts, D. A. (2003, March). The effects of vegetation phenology on endmember selection and species mapping in Southern California chaparral. *Remote Sensing of Environment, 87*(2–3), 295–309

Devore, J. L. (2000). *Probability and statistics for engineering and the sciences*. Pacific Grove, CA: Duxbury.

Dimitrakopoulos, A. P., & Bemmerzouk, A. M. (2003). Predicting live herbaceous moisture content from a seasonal drought index. *International Journal of Biometeorology*, *47*, 73–79.

Gao, B. C. (1996). NDWI—a normalized difference water index for remote sensing of vegetation liquid water from space. *Remote Sensing of Environment*, *58*, 257–266.

Gao, B. C., & Goetz, A. F. H. (1995). Retrieval of equivalent water thickness and information related to biochemical components of vegetation canopies from AVIRIS data. *Remote Sensing of Environment*, *52*, 155–162.

Green, R.O. (2003). Understanding the three phases of water with imaging spectroscopy in the solar reflected energy spectrum. Dissertation. University of California Santa Barbara, Santa Barbara, CA.

Green, R. O., Conel, J. E., Margolis, J. S., Bruegge, C. J., & Hoover, G. L. (1991). An inversion algorithm for retrieval of atmospheric and leaf water absorption from AVIRIS radiance with compensation for atmospheric scattering. *Proceedings of the Third Annual Airborne Geosciences Workshop* (pp. 51–61). Pasadena, CA: Jet Propulsion Laboratory.

Green, R., Conel, J., & Roberts, D. (1993). Estimation of aerosol optical depth and additional atmospheric parameters for the calculation of apparent surface reflectance from radiance as measured by the Airborne Visible–Infrared Imaging Spectrometer (AVIRIS). *Summaries of the Fourth Annual JPL Airborne Geosciences Workshop* (pp. 73–76). Pasadena, CA: Jet Propulsion Laboratory.

Green, R. O., Eastwood, M. L., Sarture, C. M., Chrien, T. G., Aronsson, M., Chippendale, B. J., Faust, J. A., Pavri, B. E., Chovit, C. J., Solis, M., Olah, M. R., & Williams, O. (1998). Imaging spectroscopy and the Airborne Visible/Infrared Imaging Spectrometer (AVIRIS). *Remote Sensing of Environment*, *65*, 227–248.

Jacquemoud, S., Ustin, S. L., Verdebout, J., Schmuck, G., Andreoli, G., & Hosgood, B. (1996). Estimating leaf biochemistry using the PROSPECT leaf optical properties model. *Remote Sensing of Environment*, *56*, 194–202.

Keetch, J. J., & Byram, G. M. (1968). A drought index for forest fire control. U.S. Dept. of Agriculture, forest service research paper SE-38. Southeastern Forest Experiment Station, Asheville, NC.

Peñuelas, J., Pinol, J., Ogaya, R., & Filella, I. (1997). Estimation of plant water concentration by the reflectance water Index WI (R900/R970). *International Journal of Remote Sensing*, *18*, 2869–2875.

Philpot, C. (1977). Vegetative features as determinants of fire frequency and intensity. *Symposium on Environmental Consequences of Fire and Fuel Management in Mediterranean Ecosystems* (pp. 12–16). Washington, DC: USDA Forest Service.

Pyne, S. J., Andrews, P. L., & Laven, R. D. (1996). *Introduction to wildland fire*. New York: Wiley.

Riggan, P. J., Goode, S., Jacks, P. M., & Lockwood, R. N. (1988). Interaction of fire and community development in chaparral of southern California. *Ecological Monographs*, *58*, 155–176.

Roberts, D. A., Brown, K. J., Green, R., Ustin, S., & Hinckley, T. (1998). Investigating the relationship between liquid water and leaf area in clonal Populus. *Summaries of the Seventh Airborne Earth Science Workshop* (pp. 335–344). Pasadena, CA: Jet Propulsion Laboratory.

Roberts, D. A., Green, R. O., & Adams, J. B. (1997). Temporal and spatial patterns in vegetation and atmospheric properties from AVIRIS. *Remote Sensing of Environment*, *62*, 223–240.

Serrano, L., Ustin, S. L., Roberts, D. A., Gamon, G. A., & Penuelas, J. (2000). Deriving water content of chaparral vegetation from AVIRIS data. *Remote Sensing of Environment*, *74*, 570–581.

Sims, D. A., & Gamon, J. A. (2003). Estimation of vegetation water content and photosynthetic tissue area from spectral reflectance: A comparison of indices based on liquid water and chlorophyll absorption features. *Remote Sensing of Environment*, *84*, 526–537.

Snyder, R., & Pruitt, W. (1992). Evapotranspiration data management in California. In T. Engman (Ed.), *Irrigation and drainage: Saving a threatened resource—In search of solutions* (pp. 128–133). New York: American Society of Civil Engineers.

Ustin, S. L., Roberts, D. A., Pinzon, J., Jacquemoud, S., Gardner, M., Scheer, G., Castaneda, C. M., & Palacios-Orueta, A. (1998). Estimating canopy water content of chaparral shrubs using optical methods. *Remote Sensing of Environment*, *65*, 280–291.

Zarco-Tejada, P. J., Rueda, C. A., & Ustin, S. L. (2003). Water content estimation in vegetation with MODIS reflectance data and model inversion methods. *Remote Sensing of Environment*, *85*, 109–124.

Zhang, X. Y., Friedl, M. A., Schaaf, C. B., Strahler, A. H., Hodges, J. C. F., Gao, F., Reed, B. C., & Huete, A. (2003). Monitoring vegetation phenology using MODIS. *Remote Sensing of Environment*, *84*, 471–475.